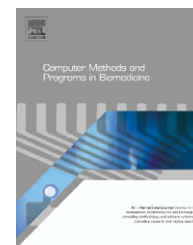




ELSEVIER

journal homepage: www.intl.elsevierhealth.com/journals/cmpb

Improving brain tumor characterization on MRI by probabilistic neural networks and non-linear transformation of textural features

Pantelis Georgiadis^{a,*}, Dionisis Cavouras^b, Ioannis Kalatzis^b, Antonis Daskalakis^b, George C. Kagadis^b, Koralia Sifaki^c, Menelaos Malamas^c, George Nikiforidis^a, Ekaterini Solomou^d

^a Medical Image Processing and Analysis (MIPA) Group, Laboratory of Medical Physics, School of Medicine, University of Patras, Rio GR-26503, Greece

^b Medical Image and Signal Processing Laboratory, Department of Medical Instrumentation Technology, Technological Education Institution of Athens, Ag. Spyridonos Street, Aigaleo GR-12210, Athens, Greece

^c 251 General Hellenic Airforce Hospital, MRI Unit, Katehaki, Athens, Greece

^d Department of Radiology, School of Medicine, University of Patras, Rio GR-26503, Greece

ARTICLE INFO

Article history:

Received 24 January 2007

Received in revised form

12 October 2007

Accepted 13 October 2007

Keywords:

Brain tumors

MRI

Textural features

Pattern classification

ABSTRACT

The aim of the present study was to design, implement and evaluate a software system for discriminating between metastatic and primary brain tumors (gliomas and meningiomas) on MRI, employing textural features from routinely taken T1 post-contrast images. The proposed classifier is a modified probabilistic neural network (PNN), incorporating a non-linear least squares features transformation (LSFT) into the PNN classifier. Thirty-six textural features were extracted from each one of 67 T1-weighted post-contrast MR images (21 metastases, 19 meningiomas and 27 gliomas). LSFT enhanced the performance of the PNN, achieving classification accuracies of 95.24% for discriminating between metastatic and primary tumors and 93.48% for distinguishing gliomas from meningiomas. To improve the generalization of the proposed classification system, the external cross-validation method was also used, resulting in 71.43% and 81.25% accuracies in distinguishing metastatic from primary tumors and gliomas from meningiomas, respectively. LSFT improved PNN performance, increased class separability and resulted in dimensionality reduction.

© 2007 Elsevier Ireland Ltd. All rights reserved.

1. Introduction

According to a recent statistical report published by the Central Brain Tumor Registry of the United States (CBTRUS), approximately 39,550 people were newly diagnosed with primary benign and primary malignant brain tumors [1,2] in 2002 [3]. Furthermore, in 2000, more than 81,000 people, in

the United States alone, were living with a primary malignant brain tumor and 267,000 were living with a primary benign brain tumor. The same report indicates that the incidence rate of primary brain tumors, whether benign or malignant, is 14 per 100,000, while median age at diagnosis is 57 years [3].

Secondary or metastatic brain tumors [1], in contrast to primary brain tumors, originate in tissues outside the central

* Corresponding author. Tel.: +30 2610 997745.

E-mail addresses: pgeorgiadis@med.upatras.gr (P. Georgiadis), cavouras@teiath.gr (D. Cavouras).

URL: <http://mipa.med.upatras.gr/> (P. Georgiadis).

0169-2607/\$ – see front matter © 2007 Elsevier Ireland Ltd. All rights reserved.

doi:10.1016/j.cmpb.2007.10.007

nervous system and are a common complication of systemic cancer. Brain metastases outnumber primary brain tumors and are currently classified as the most frequent intracranial tumors. Other studies indicate that brain metastases occur in 20–40% of all cancer patients and that more than 100,000 individuals per year will develop brain metastases [3].

Today, imaging techniques, like magnetic resonance imaging (MRI), are used to locate the position and extent of brain tumors. MRI can provide information about brain tissues, from a variety of excitation sequences. Compared with other diagnostic imaging modalities, such as computerized tomography, MRI provides superior contrast for different brain tissues [4]. Additionally, MR images encapsulate valuable information regarding numerous tissue parameters (proton density, spin–lattice (T1) and spin–spin (T2) relaxation times, flow velocity and chemical shift), which lead to more accurate brain tissue characterization. These unique advantages have characterized MRI as the method of choice in brain tumor studies [5].

Brain tumor characterization is a process that requires a complicated assessment of the various MR image features and is typically performed by experienced radiologists. An expert radiologist performs this task with a significant degree of precision and accuracy, despite the inherently subjective nature of many of the decisions associated with this process. Nevertheless, in the effort to deliver more effective treatment, clinicians are continuously seeking for greater accuracy in the pathological characterization of brain tissues from imaging investigations [6].

2. Background and design considerations

To this need, image analysis techniques have been employed in previous studies for the extraction of diagnostic information from MR images [6–8]. These studies have employed pattern recognition and texture analysis techniques to characterize human brain tumors. In a recent study [9], an SVM-based classification system has achieved 95% overall accuracy in discriminating between gliomas and meningiomas. In another study [7], the hierarchical ascending classification with correspondence factorial analysis has been used for discriminating between different tumor types, with accuracies ranging between 49% (tumors versus oedemas) and 63% (benign versus malignant tumors). In a previous study [6], discriminant analysis and the k-nearest neighbor classifier have been adopted for distinguishing between human brain tumors and oedematous tissues, achieving maximum overall accuracy of 95%. In another study [10], several non-pictorial diagnostic factors, such as age, oedema, blood supply, calcification and haemorrhage, that were employed in an SVM classification scheme, have been found to be important in assessing brain gliomas. Finally, more recent studies have employed MR spectroscopic features [11–16] or combination of textural and spectroscopic features to discriminate between various types of brain tumors achieving accuracies up to 99% [15]. These studies, utilizing either statistical analysis techniques or state of art classifiers, have shown that MR spectroscopic features can provide an added value in the accurate characterization of brain tumors. However, obtaining of MR spectroscopy data is

not a readily available function in all MRI units and additionally it requires expertise for signal conditioning.

The aim of the present study was to design, implement and evaluate a pattern recognition system, which, by analyzing routinely taken T1 post-contrast MR images, would improve brain tumor classification accuracy. Employing a two-level hierarchical decision tree, distinction between metastatic and primary brain tumors and between gliomas and meningiomas were performed at the first and second level of the decision tree, respectively. Additionally, the present study demonstrated that by employing textural features from MR images and by conditioning those features by means of a non-linear least squares features transformation (LSFT), the performance of the probabilistic neural network (PNN) classifier was boosted significantly.

3. System description

3.1. Data acquisition

A total number of 67 T1-weighted gadolinium-enhanced MR images were obtained from the Hellenic Airforce Hospital with verified intracranial tumors, using a SIEMENS-Sonata 1.5 Tesla MR Unit. The image dataset comprised 21 metastases, 19 meningiomas and 27 gliomas. From each case, only T1-weighted post-contrast (Gadolinium) images, with spin echo (SE) sequence, echo time (TE = 15 ms) and repetition time (TR = 500 ms), were used for further analysis. The reason for employing T1 post-contrast images is the increased diagnostic information that they encapsulate in comparison to pre-contrast T1 or T2 weighted images. More specifically, contrast administration assists in the separation of tumor from oedema improving visualization, localization and tumor margin delineation. Contrast enhancement is intense because of the hi-degree of blood brain barrier (BBB) disruption [17].

Transverse images were selected through the tumor's center by an expert radiologist (M.M.).

3.2. Feature extraction and reduction

Utilizing these images, the radiologist specified square regions of interest (ROIs) within the tumor area. Each ROI was semi-automatically drawn around a pixel by a simple click on the mouse. From each ROI, a series of 36 features were extracted; 4 features from the ROI's histogram, 22 from the co-occurrence matrices [18] and 10 from the run-length matrices [19].

All features were normalized to zero mean and unit standard deviation [20], according to relation (1)

$$x'_i = \frac{x_i - m}{std}, \quad (1)$$

where x_i and x'_i are the i th feature values before and after the normalization, respectively, and m and std are the mean value and standard deviation, respectively, of feature x_i over all patterns and all classes. Regarding the latter, only 2-class classification problems (primary versus secondary and gliomas versus meningiomas) were considered, embedded in a two-level hierarchical decision-tree structure. In order to reduce feature dimensionality, the non-parametric Wilcoxon rank-

The dimensionality of the extended pattern vector ($\hat{\mathbf{x}}$) is equal to [20]:

$$\hat{d} = \frac{(d+n)!}{d!n!} - 1. \tag{4}$$

For the formulation of a LSFT 2-class problem, let space S , with dimensionality equal to the number of classes ($K=2$), and let $P_i = [p_{i1} p_{i2}]$, $i = 1, 2$ be arbitrary defined points in space S , corresponding to each class i . A transformation T is sought such that the total mean square error between the transformed extended vectors ($T\hat{\mathbf{x}}_{ij}$) and P_i is minimized as follows (assuming equal a priori probabilities for each class i):

$$\nabla_T \left[\sum_{i=1}^K \left(\frac{1}{N_i} \sum_{j=1}^{N_i} (T\hat{\mathbf{x}}_{ij} - P_i)' (T\hat{\mathbf{x}}_{ij} - P_i) \right) \right] = 0, \tag{5}$$

or

$$\sum_{i=1}^K \left(\frac{1}{N_i} \sum_{j=1}^{N_i} [\nabla_T(\hat{\mathbf{x}}'_{ij} T' T \hat{\mathbf{x}}_{ij}) - 2 \nabla_T(\hat{\mathbf{x}}'_{ij} T' P_i) + \nabla_T(P_i P_i)] \right) = 0 \tag{6}$$

where K is the number of classes, N_i is the number of patterns of class i and $\hat{\mathbf{x}}_{ij}$ are the n -degree extended training patterns of class i . Applying basic matrix algebra to the terms of (6):

$$\nabla_T(\hat{\mathbf{x}}'_{ij} T' T \hat{\mathbf{x}}_{ij}) = 2T(\hat{\mathbf{x}}_{ij} \hat{\mathbf{x}}'_{ij}) \tag{7}$$

$$\nabla_T(\hat{\mathbf{x}}'_{ij} T' P_i) = P_i \hat{\mathbf{x}}'_{ij} \tag{8}$$

$$\nabla_T(P_i P_i) = 0 \tag{9}$$

Eqs. (6)–(9) give:

$$\sum_{i=1}^K \left(\frac{1}{N_i} \sum_{j=1}^{N_i} [2T(\hat{\mathbf{x}}_{ij} \hat{\mathbf{x}}'_{ij}) - 2P_i \hat{\mathbf{x}}'_{ij}] \right) = 0 \tag{10}$$

or

$$T \sum_{i=1}^K \left(\frac{1}{N_i} \sum_{j=1}^{N_i} \hat{\mathbf{x}}_{ij} \hat{\mathbf{x}}'_{ij} \right) - \sum_{i=1}^K \left(\frac{1}{N_i} \sum_{j=1}^{N_i} P_i \hat{\mathbf{x}}'_{ij} \right) = 0 \tag{11}$$

which results in:

$$T = \left[\sum_{i=1}^K \left(\frac{1}{N_i} \sum_{j=1}^{N_i} P_i \hat{\mathbf{x}}'_{ij} \right) \right] \left[\sum_{i=1}^K \left(\frac{1}{N_i} \sum_{j=1}^{N_i} \hat{\mathbf{x}}_{ij} \hat{\mathbf{x}}'_{ij} \right) \right]^{-1} \tag{12}$$

Transformation matrix T is a $K \times \hat{d}$ matrix, so the decision space dimensionality is equal to the number of brain tumor classes.

Following the LSFT procedure, patterns $\hat{\mathbf{x}}_{ij}$ were fed into the PNN classifier, resulting in the final discriminant function of

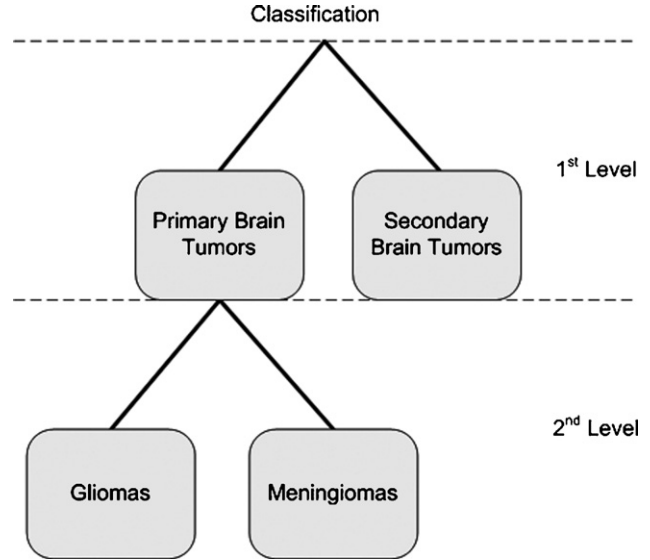


Fig. 2 – Hierarchical tree classification scheme.

the LSFT-PNN classifier:

$$g_i(\mathbf{x}) = \frac{1}{(2\pi)^{\hat{d}/2} \sigma^{\hat{d}}} \frac{1}{N_i} \sum_{j=1}^{N_i} \exp \left[-\frac{(T\hat{\mathbf{x}} - T\hat{\mathbf{x}}_{ij})'(T\hat{\mathbf{x}} - T\hat{\mathbf{x}}_{ij})}{2\sigma^2} \right]. \tag{13}$$

3.4. Design of the classification scheme

A two level hierarchical decision tree was designed to discriminate the metastatic brain tumor cases from the gliomas and meningiomas (primary brain tumors) cases (Fig. 2). At the first level, the gliomas and the meningiomas cases were grouped into the primary brain tumor class and were classified against the metastatic brain tumor cases. At the second level, the primary tumor cases were further classified into cases with gliomas and meningiomas.

At each level, classification was performed using two different LSFT-PNN classifiers. At the first level of the decision tree, a third degree (cubic) LSFT-PNN ($k=3$ in Eq. (3)) was employed to discriminate between primary and metastatic tumors while, at the second level, a second degree (quadratic) LSFT-PNN ($k=2$ in Eq. (3)) was used to classify gliomas and meningiomas. The choice of the classifier's degree was made on the basis of optimal classification, following a multiple experimentation procedure.

Prior to entering the classification system, each classifier was optimized employing the available dataset. Optimization was performed, separately at both levels of the decision tree, by exhaustively combining (in all possible combinations of 2, 3, etc., features) the statistically reduced feature vectors (10 features of high discriminatory power ($p < 0.001$) were retained) and by using the leave-one-out method (LOO) [16], for assessing the performance of each feature combination.

To avoid overfitting conditions, which may occur by using the same dataset in the feature selection and system evaluation stages, the external cross-validation (ECV) method [24] was also used. Accordingly, the dataset was split in two sets, one was used for optimum classifier design (2/3 of the dataset)

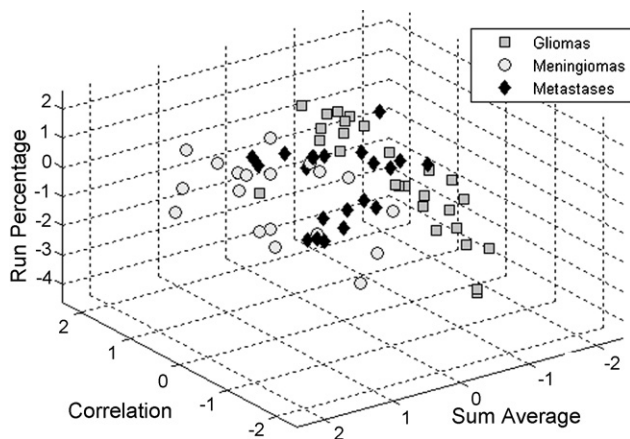


Fig. 3 – Scatter diagram of the classes involved.

and the other for evaluation (1/3 of the dataset). Optimum classifier design was achieved by employing: (i) the Wilcoxon non-parametric test for feature reduction and (ii) the LOO and exhaustive search methods for determining the highest classification accuracy with the least number of features. That optimum classifier design was next used to classify the evaluation subset. This cycle (design-classification) was repeated ten times, each time picking the training subset randomly and forming the evaluation subset by the remaining data. Finally, classification accuracy results were averaged for assessing the generalization performance of the proposed method.

This type of classifier training required several hours of processing time, while classification time, once the system has been trained, was infinitesimal. The overall accuracy of the classification system, in discriminating metastatic brain tumors from gliomas and meningiomas cases, was determined by multiplying the system’s performance at each level [20].

4. Experimental results

Fig. 3 shows a scatter diagram of the classes involved. The complexity of the problem has led us to adopt a hierarchical decision tree structure (see Fig. 2). The overall classification accuracy at the first level of the decision tree was 94.03% employing the cubic LSFT-PNN classifier. Individual accuracies in discriminating between primary and secondary brain tumors were 93.48% and 95.24%, respectively (Table 1). Best feature vector, used for the optimal design of the cubic LSFT-PNN classifier, comprised the mean value, entropy, and

Table 1 – Cubic LSFT-PNN classifier truth table for discriminating primary and secondary tumors

	Primary brain tumors	Secondary brain tumors	Accuracy (%)
Primary brain tumors	43	3	93.48
Secondary brain tumors	1	20	95.24
Overall accuracy			94.03

Table 2a – Classification results for discriminating primary and secondary brain tumors employing the LOO method

	Primary brain tumors accuracy (%)	Secondary brain tumors accuracy (%)	Overall accuracy (%)
PNN	86.96	95.24	89.55
Linear LSFT-PNN	89.13	95.24	91.04
SVM-RBF	91.30	85.71	89.55
ANN	95.65	95.24	95.52
Cubic LSFT-PNN	93.48	95.24	94.03

Table 2b – Classification results for discriminating primary and secondary brain tumors utilizing the ECV method (averaged results after ten repetitions)

	Primary brain tumors accuracy (%)	Secondary brain tumors accuracy (%)	Overall accuracy (%)
PNN	84.38	52.86	74.78
Linear LSFT-PNN	89.38	37.14	73.48
SVM-RBF	93.75	30.00	74.35
ANN	88.13	61.43	80.00
Cubic LSFT-PNN	81.25	71.43	78.26

difference entropy. Employing the ECV method, the mean overall accuracy of the cubic LSFT-PNN classifier was 78.26%, while the mean accuracies for primary and secondary brain tumors discrimination were 81.25% and 71.43%, respectively.

The performance of the cubic LSFT-PNN algorithm, used at the first level of the decision tree, was tested against the PNN, the linear LSFT-PNN, the Support Vector Machines with Radial Basis Function kernel (SVM-RBF) and the Artificial Neural Network (ANN) classifiers, which were trained in a similar manner to the cubic LSFT-PNN classifier. Comparative classification results employing the LOO and the ECV methods are presented in Tables 2a and 2b, respectively, as well as in Fig. 4.

Figs. 5–8 show scatter diagrams displaying primary and secondary tumor class separation for the cubic LSFT-PNN, the PNN, the SVM-RBF and the ANN classifiers.

At the second level of the decision tree, employing the quadratic LSFT-PNN classifier, discrimination accuracy

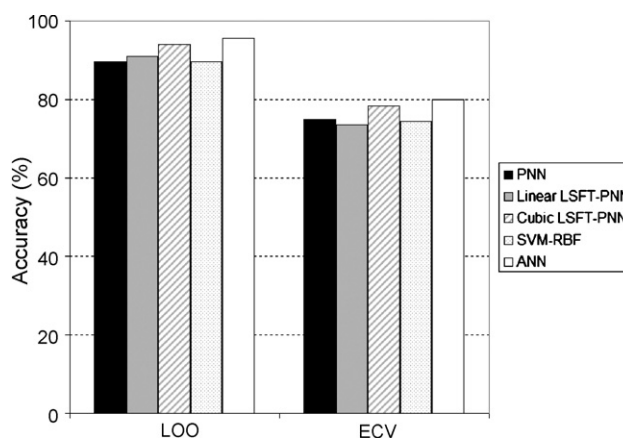


Fig. 4 – Overall classification accuracy of the algorithms used for discriminating primary and secondary tumors.

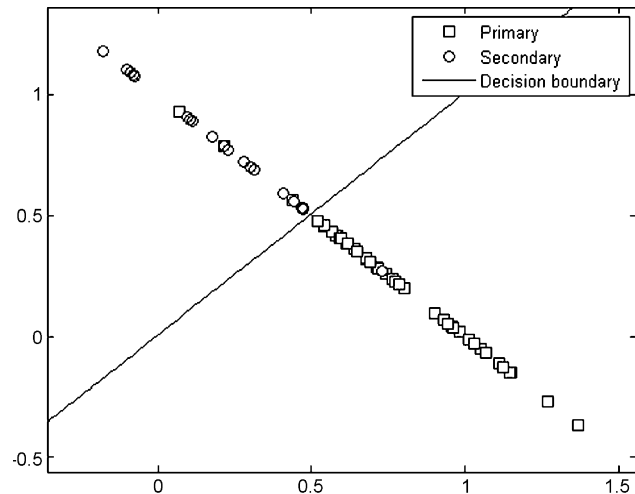


Fig. 5 – Scatter diagram of the optimum feature combination of the cubic LSFT-PNN classifier and the corresponding decision boundary for discriminating primary and secondary tumors.

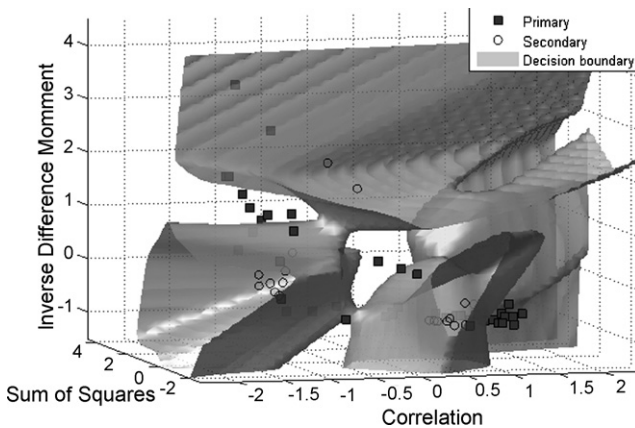


Fig. 6 – Scatter diagram of the optimum feature combination of the PNN classifier and the corresponding decision boundary for discriminating primary and secondary tumors.

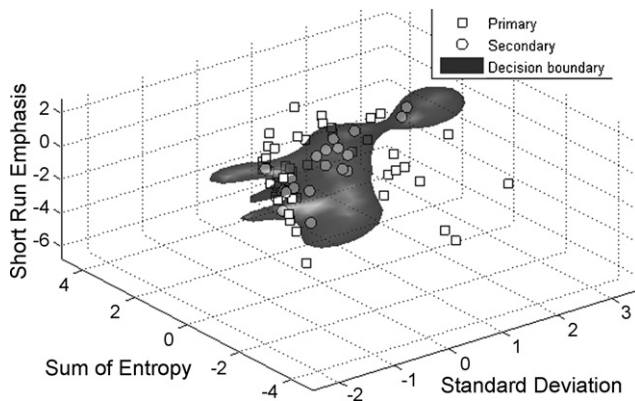


Fig. 7 – Scatter diagram of the optimum feature combination of the SVM-RBF classifier and the corresponding decision boundary for discriminating primary and secondary tumors.

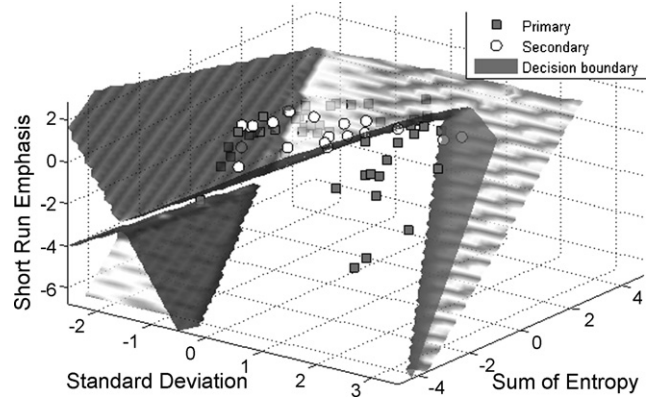


Fig. 8 – Scatter diagram of the optimum feature combination of the ANN classifier and the corresponding decision boundary for discriminating primary and secondary tumors.

between the two types of primary brain tumors (gliomas and meningiomas) was 100% (Table 3). The best feature vector, employed for the optimal design of the quadratic LSFT-PNN classifier, comprised the mean value, angular second moment and the inverse difference moment. Utilizing the ECV technique, the mean overall accuracy of the quadratic LSFT-PNN classifier was 99.33%, while the mean accuracies for gliomas and meningiomas discrimination were 88.89% and 100%, respectively.

The classification accuracy of the quadratic LSFT-PNN classification scheme, used at the second level of the decision tree, was tested against that of the PNN, the linear LSFT-PNN, the SVM-RBF and the ANN classifiers. Both PNN and linear LSFT-PNN misclassified one glioma case resulting in 97.83% overall accuracy while SVM-RBF and ANN classifiers achieved overall discrimination accuracy of 100% and 93.43%, respectively (Tables 4a and 4b) (Fig. 9).

Table 3 – Quadratic LSFT-PNN truth table for discriminating gliomas and meningiomas

	Gliomas	Meningiomas	Accuracy (%)
Gliomas	27	0	100
Meningiomas	0	19	100
Overall accuracy			100

Table 4a – Classification results for discriminating gliomas and meningiomas employing the LOO method

	Gliomas accuracy (%)	Meningiomas accuracy (%)	Overall accuracy (%)
PNN	96.30	100	97.83
Linear LSFT-PNN	96.30	100	97.83
SVM-RBF	100	100	100
ANN	92.59	94.74	93.43
Quadratic LSFT-PNN	100	100	100

Table 4b – Classification results for discriminating gliomas and meningiomas utilizing the ECV method (averaged results after ten repetitions)

	Gliomas accuracy (%)	Meningiomas accuracy (%)	Overall accuracy (%)
PNN	94.44	85.00	90.67
Linear LSFT-PNN	90.00	86.67	88.67
SVM-RBF	100	43.33	77.33
ANN	94.44	83.33	90
Quadratic LSFT-PNN	88.89	100	99.33

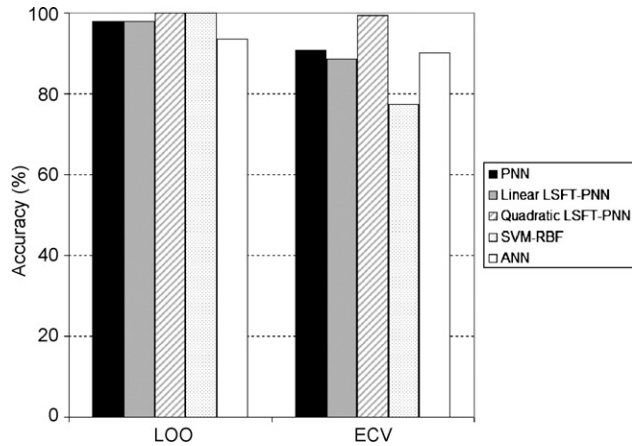


Fig. 9 – Overall classification accuracy of the algorithms used for discriminating gliomas and meningiomas.

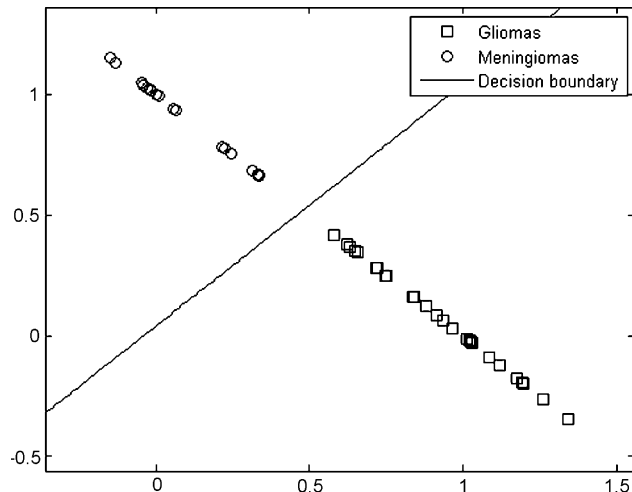


Fig. 10 – Scatter diagram of the optimum feature combination of the quadratic LSFT-PNN classifier and the corresponding decision boundary for discriminating gliomas and meningiomas.

Figs. 10–13 show scatter diagrams displaying gliomas and meningiomas class separation employing the quadratic LSFT-PNN, PNN, SVM-RBF and ANN classifiers.

The overall accuracies of the classification system in discriminating metastatic tumors from gliomas and menin-

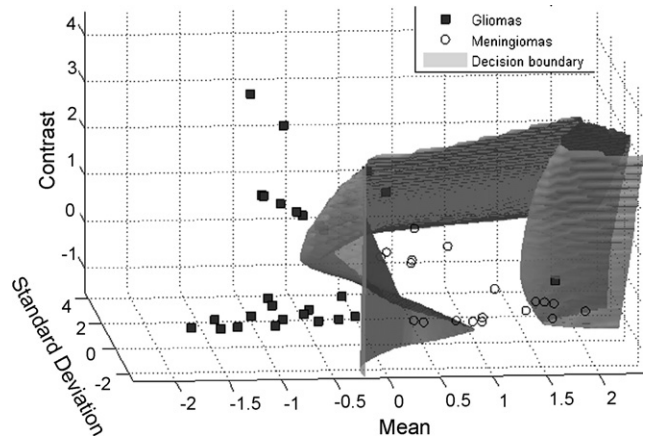


Fig. 11 – Scatter diagram of the optimum feature combination of the PNN classifier and the corresponding decision boundary for discriminating gliomas and meningiomas.

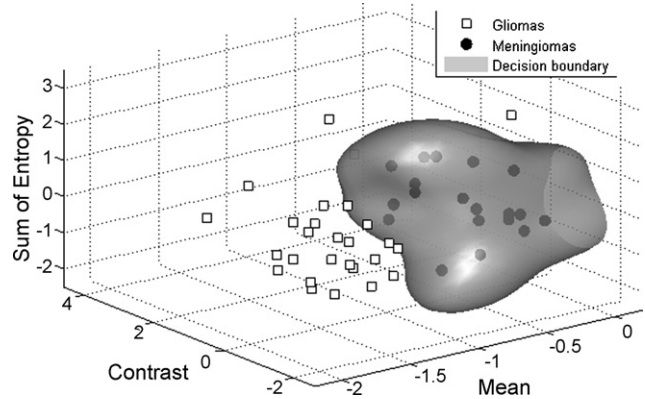


Fig. 12 – Scatter diagram of the optimum feature combination of the SVM-RBF classifier and the corresponding decision boundary for discriminating gliomas and meningiomas.

gliomas can be obtained by multiplying the corresponding accuracies achieved at each level of the decision tree [20]. Consequently, classification accuracies were 95.24% for the metastatic and 93.48% for both gliomas and meningiomas brain tumor cases, while employing the ECV method the classification accuracies were 71.43% for the metastatic, 72.22% for gliomas and 81.25% for meningiomas.

5. Discussion

The LSFT-PNN and the PNN classification schemes were optimized with respect to parameter settings and available feature data. The spread of Gaussian function for the LSFT-PNN and the PNN classifiers was experimentally set equal to $\sigma = 0.3$.

In accordance with our findings, the LSFT-PNN outperformed the PNN at both levels of the decision tree. At the first level, the LSFT-PNN achieved a sensitivity of 93.48% against PNN's 86.96% in correctly characterizing primary tumors, assigning three more primary brain tumors to the appropriate

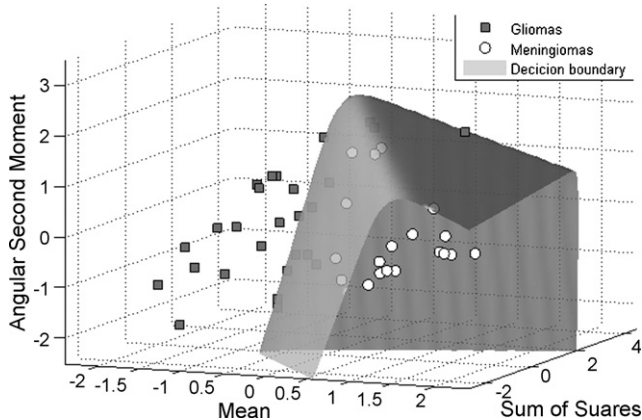


Fig. 13 – Scatter diagram of the optimum feature combination of the ANN classifier and the corresponding decision boundary for discriminating gliomas and meningiomas.

class. This is important, since the precision of such a decision may be crucial in patient management.

On the other hand, the specificity achieved by both classifiers in assigning the metastatic brain tumors to the correct classes was the same (95.24%), both missing out only one secondary brain tumor. Again, this is of value since metastatic tumors require specific treatment protocols, such as radiation therapy and chemotherapy, while primary tumors may also require surgical intervention [25,26]. The best features combination of the cubic LSFT-PNN classifier, at the first level of the decision tree, expresses the signal strength (mean value) and the degree of the in-homogeneity (entropy and difference entropy) in the gray-tones of the ROIs. In a previous study [13] employing only MR spectroscopic data and the LS-SVM classification algorithm, precisions in distinguishing between metastatic brain tumors and meningiomas or glioblastomas or astrocytomas were 97%, 59% and 96%, respectively. Our findings are comparable, however employing solely textural features from the T1-contrast enhanced MR images.

At the second level of the decision tree, the quadratic LSFT-PNN discriminated correctly all gliomas and meningiomas cases while the PNN classifier failed to classify correctly one glioma case. The best features combination of the quadratic LSFT-PNN expresses the signal strength (mean value) and a measure of the homogeneity (angular second moment and inverse difference moment) in the gray-tones of the ROIs [18]. These textural characteristics are related to textural parameters that physicians employ in diagnosis and they are proportional to the textural imprint of these two types of brain tumors, i.e. gliomas have heterogeneous texture while meningiomas appear to be homogeneous in MR imaging. In a recent study [9], an SVM-based classification system achieved 95% overall accuracy in discriminating between gliomas and meningiomas, employing as features image intensities from four sequences (T1, T2, PD, GD). When MR spectra from the lesions were also included as features, classification accuracy reached 99.8%. These results are comparable with our findings regarding discrimination between gliomas and meningiomas (Table 3), where we have employed solely textural features from T1 post-contrast MR images.

Considering the results, it can be claimed that the non-linear LSFT-PNN outperforms the PNN and the linear LSFT-PNN. This may be attributed to the increased class separability that the LSFT procedure provides, especially when non-linear terms are introduced in the classifier's discriminant function. Another advantage of the LSFT-PNN is the dimensionality reduction, equal to the number of classes, independently of the number of features, which leads to more robust classification. The computational requirements of the LSFT-PNN classifier are comparable to those of the PNN, as the additional time required to perform the LSFT procedure is gained in the classification step, due to the reduced dimensionality of the problem.

Additionally, the proposed non-linear LSFT-PNN algorithm was compared against the SVM-RBF and the ANN classifiers at both levels of the hierarchical decision tree. Judging from the results, the proposed algorithm achieved higher discrimination accuracies than the SVM-RBF, at both levels of the decision tree, while its precision was close to the ANN classifier in discriminating primary from secondary tumors. However, it must be noted that both SVM-RBF and ANN classifiers required a significant amount of processing time in their training stage. The computational times required for the training and evaluation procedures (10 repetitions of ECV employing LOO and exhaustive search) were, approximately, 40 min for the proposed LSFT-PNN algorithm, 16 h for the SVM-RBF classifier and 11 h for the ANN classifier (employing the sequential forward selection technique [20], since the exhaustive search was unrealistically time demanding for the ANN). This may be attributed to their internal optimization procedures, i.e. the sequential optimization procedure for the SVM-RBF and the back-propagation procedure for the ANN. On the other hand, the proposed algorithm does not require optimization, rendering the classification system fast and efficient in its training.

Employing the ECV method, the overall and individual discrimination accuracies were decreased. However, the adoption of this method rendered the system more general in its behavior regarding the classification of new datasets. The overall discrimination accuracy decrement using the ECV method was in accordance with [24]. The determination of a unique best feature vector was not possible employing the ECV technique as, at each repetition, different feature vectors were produced. However, most of those features were related to texture homogeneity of the ROIs.

Acknowledgement

Funding by the University of Patras Research Committee under the basic research program “K. Karatheodori”, project title “Computer Assisted Diagnosis of Brain Tumors based on Statistical Methods and Pattern Recognition Techniques” is gratefully acknowledged.

REFERENCES

- [1] L.S. Ashby, M.M. Troester, W.R. Shapiro, Central nervous system tumors, *Update Cancer Therapeut.* 1 (4) (2006) 475–513.

- [2] G. Cruickshank, Tumours of the brain, Surgery (Oxford) 22 (3) (2004) 69–72.
- [3] N.D. Doolittle, State of the science in brain tumor classification, Semin. Oncol. Nurs. 20 (4) (2004) 224–230.
- [4] S. Shen, W. Sandham, M. Granat, A. Sterr, MRI fuzzy segmentation of brain tissue using neighborhood attraction with neural-network optimization, IEEE Trans. Inf. Technol. Biomed. 9 (3) (2005) 459–467.
- [5] H. Soltanian-Zadeh, D.J. Peck, J.P. Windham, T. Mikkelsen, Brain tumor segmentation and characterization by pattern analysis of multispectral NMR images, NMR Biomed. 11 (4–5) (1998) 201–208.
- [6] R.A. Lerski, K. Straughan, L.R. Schad, D. Boyce, S. Bluml, I. Zuna, MR image texture analysis—an approach to tissue characterization, Magn. Reson. Imaging 11 (6) (1993) 873–887.
- [7] S. Herlidou-Meme, J.M. Constans, B. Carsin, D. Olivie, P.A. Eliat, L. Nadal-Desbarats, et al., MRI texture analysis on texture test objects, normal brain and intracranial tumors, Magn. Reson. Imaging 21 (9) (2003) 989–993.
- [8] L.R. Schad, S. Bluml, I. Zuna, MR tissue characterization of intracranial tumors by means of texture analysis, Magn. Reson. Imaging 11 (6) (1993) 889–896.
- [9] A. Devos, A.W. Simonetti, M. van der Graaf, L. Lukas, J.A. Suykens, L. Vanhamme, et al., The use of multivariate MR imaging intensities versus metabolic data from MR spectroscopic imaging for brain tumour classification, J. Magn. Reson. 173 (2) (2005) 218–228.
- [10] G.-Z. Li, J. Yang, C.-Z. Ye, D.-Y. Geng, Degree prediction of malignancy in brain glioma using support vector machines, Comput. Biol. Med. 36 (3) (2006) 313–325.
- [11] C. Majos, M. Julia-Sape, J. Alonso, M. Serrallonga, C. Aguilera, J.J. Acebes, et al., Brain tumor classification by proton MR spectroscopy: comparison of diagnostic accuracy at short and long TE, AJNR Am. J. Neuroradiol. 25 (10) (2004) 1696–1704.
- [12] L. Lukas, A. Devos, J.A. Suykens, L. Vanhamme, F.A. Howe, C. Majos, et al., Brain tumor classification based on long echo proton MRS signals, Artif. Intell. Med. 31 (1) (2004) 73–89.
- [13] A. Devos, L. Lukas, J.A. Suykens, L. Vanhamme, A.R. Tate, F.A. Howe, et al., Classification of brain tumours using short echo time 1H MR spectra, J. Magn. Reson. 170 (1) (2004) 164–175.
- [14] Y. Huang, P.J.G. Lisboa, W. El-Deredy, Tumour grading from magnetic resonance spectroscopy: a comparison of feature extraction with variable selection, Statist. Med. 22 (1) (2003) 147–164.
- [15] A.R. Tate, C. Majos, A. Moreno, F.A. Howe, J.R. Griffiths, C. Arus, Automated classification of short echo time in vivo 1H brain tumor spectra: a multicenter study, Magn. Reson. Med. 49 (1) (2003) 29–36.
- [16] Y.-D. Cho, G.-H. Choi, S.-P. Lee, J.-K. Kim, 1H-MRS metabolic patterns for distinguishing between meningiomas and other brain tumors, Magn. Reson. Imaging 21 (6) (2003) 663–672.
- [17] V. Runge, Brain: neoplastic disease, in: Clinical MRI, Saunders, Philadelphia, 2002.
- [18] R.M. Haralick, K. Shanmugam, I. Dinstein, Textural features for image classification, IEEE Trans. Syst. Man Cybern SMC-3 (1973) 610–621.
- [19] M.M. Galloway, Texture analysis using grey level run lengths, Comp. Graph. Image Proc. 4 (1975) 172–179.
- [20] S. Theodoridis, K. Koutroumbas, System evaluation, in: Pattern Recognition, Academic Press, UK, 1998.
- [21] F. Wilcoxon, Individual comparisons by ranking methods, Biometrics 1 (1945) 80–83.
- [22] D.F. Specht, Probabilistic neural networks, Neural Networks 3 (1990) 109–118.
- [23] N. Ahmed, R. Rao, Feature selection in pattern recognition, in: Orthogonal Transforms for Digital Signal Processing, Springer Verlag, NY, 1975.
- [24] C. Ambroise, G.J. McLachlan, Selection bias in gene extraction on the basis of microarray gene-expression data, Proc. Natl. Acad. Sci. U.S.A. 99 (10) (2002) 6562–6566.
- [25] C.A. Graham, T.F. Cloughesy, Brain tumor treatment: chemotherapy and other new developments, Semin. Oncol. Nurs. 20 (4) (2004) 260–272.
- [26] K.H. Peacock, G.J. Lesser, Current therapeutic approaches in patients with brain metastases, Curr. Treat. Opt. Oncol. 7 (6) (2006) 479–489.